Interaction between charged anisotropic macromolecules: Application to rod-like polyelectrolytes

David Chapot
Laboratoire de Physique de l'E.N.S. de Lyon, UMR CNRS 5672, 46 Allée d'Italie, 69364 Lyon Cedex, France

Lydéric Bocquet[a)]
Laboratoire PMCN, UMR CNRS 5586, Université Lyon 1, 69622 Villeurbanne Cedex, France

Emmanuel Trizac
Laboratoire de Physique Théorique, UMR CNRS 8627, Bâtiment 210, Université Paris-Sud, 91405 Orsay Cedex, France

(Received 11 September 2003; accepted 26 November 2003)

In this paper we propose a framework allowing one to compute the effective interactions between two anisotropic macromolecules, thereby generalizing the Derjaguin, Landau, Verwey, and Overbeek theory [E. J. W. Verwey and J. T. G. Overbeek, *Theory of the Stability of Lyophobic Colloids* (Elsevier, Amsterdam, 1948)] to nonspherical finite size colloids. We show in particular that the effective interaction potential remains anisotropic at all distances and provide an expression for the anisotropy factor. We then apply this framework to the case of finite rod-like polyelectrolytes. The calculation of the interaction energy requires the numerical computation of the surface charge profiles, which result here from a constant surface potential on the rod-like colloids. However, a simplified analytical description is proposed, leading to an excellent agreement with the full numerical solution. Conclusions on the phase properties of rod-like colloids are proposed in this context. © *2004 American Institute of Physics.* [DOI: 10.1063/1.1642617]

I. INTRODUCTION

The DLVO theory, named after Derjaguin, Landau, Verwey, and Overbeek,[1] is one of the most influential and still very important descriptions of charged colloidal suspensions. It was developed more than 50 years ago to rationalize the stability of lyophobic colloidal suspensions. One specific prediction of the DLVO theory is the far-field pair potential between two spherical colloids of like radii a which, within a linearization approximation, takes a Yukawa form:

$$U_{12}(r)=\frac{Z^2e^2}{4\pi\epsilon}\left(\frac{\exp[\kappa_D a]}{1+\kappa_D a}\right)^2\frac{\exp(-\kappa_D r)}{r}, \tag{1}$$

where Z is the valence of the object, e the elementary charge, and κ_D denotes the inverse Debye screening length. The latter is defined in terms of the micro-ions bulk densities $\{\rho_\alpha\}$ (with valencies $\{z_\alpha\}$) as $\kappa_D^2=4\pi\ell_B\Sigma_\alpha\rho_\alpha z_\alpha^2$. At the level of a dielectric continuum approximation for the solvent with permittivity ϵ, the Bjerrum length ℓ_B is defined as $\ell_B=e^2/(4\pi\epsilon k_BT)$, where k_BT is the thermal energy: $\ell_B=7$ Å for water at room temperature. Note that the Debye screening factor, κ_D, does characterize the decay rate of the interaction potential in the far field region, therefore providing an experimental measurement of the screening factor from interaction force measurements (see, e.g., Ref. 2).

However, in the colloid world, the spherical shape is not the rule and many macromolecules are intrinsically very anistropic: rod-like or ribbon-like shapes (DNA molecules, TMV or fd virus, V_2O_5 ribbons, Boehmite rods, etc.),[3–7] disk-like shapes (e.g., for clays, as laponite, bentonite, etc.).[8–11] Since the seminal work of Langmuir on bentonite clay particles published in 1938,[12] these systems have been the object of considerable attention, in particular in the context of orientational phase transitions (such as isotropic to nematic I–N, etc.).[13] From the theoretical side, these transitions were first addressed by Onsager,[14] who showed that the nematic phase was stabilized at high density by purely entropic effects. The extension to charged rods has been reconsidered more recently by Stroobants *et al.*,[15] showing that the electrostatic interaction between the polyelectrolytes lead to a twisting effect which enhances the concentration at the I–N transition. The picture of Onsager correctly reproduces the experimental results for highly disymmetric particles, such as TMV or fd viruses.[3,4] However in many anisotropic systems, a gelation occurs before any I–N transition.[6,8,9] According to the DLVO theory, gelation is usually assumed to result from the presence of van der Waals attraction between the macromolecules, which overcome at high salinity the double layer repulsion. However, the origin of gelation in many rod- and platelet-like systems remains quite obscure.[6,9,16] The ''gel'' denomination is also misleading in some cases since the texture of the ''gelled'' system may be closer to a glassy like phase, in which the orientational and translational degrees of freedom are frozen.[16,17] The origin of such a glass-like transition is still under debate.

In this paper, we shall stay at a more ''microscopic'' level and consider the effects of anisotropy on the interaction between two macromolecules, much in the spirit of the

a)Electronic mail: lbocquet@lpmcn.univ-lyon1.fr

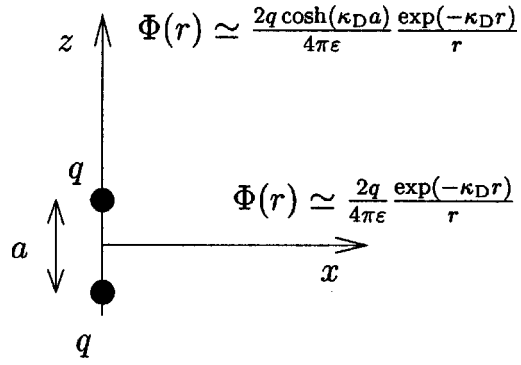

FIG. 1. Illustration of the anisotropic effect. In the x and z directions, the far-field potentials differ from a factor $\cosh(\kappa_D a)$ which does not vanish at any distance.

DLVO approach. One specific question we raise is the following. We consider two anisotropic particles, separated by a ''large'' distance (i.e., a distance r larger than their typical dimension a). Can the electrostatic interaction between these two individual objects be modeled by the previous DLVO result, i.e., is the anisotropy lost for large distances? This is of course the case in the absence of salt.[18] Does this result generalize with an electrolyte?

Before delving into the details, let us first consider a much simpler problem, namely that of two identical charges q, with positions $z=\pm a/2$ along the z axis (a fixed) and embedded in an electrolyte (1): what is the electrostatic potential ϕ created by these two charges at large distances?

Naively, one would expect that the anisotropy is lost for large distances (i.e., distances larger than the size a of the object, or larger than the Debye length $1/\kappa_D$) and the potential should reduce to its Yukawa form

$$\Phi(r)=\frac{2q}{4\pi\epsilon}\frac{\exp(-\kappa_D r)}{r}.$$

But this is actually *not* the case! This can be understood by computing—within a linear Debye–Hückel-type theory—the potential at large distances in the x and z directions: along the axis x, one gets as expected

$$\Phi(r)\simeq\frac{2q}{4\pi\epsilon}\frac{\exp(-\kappa_D r)}{r}$$

to lowest order in a/r; but on the z axis, one gets at the same order

$$\Phi(r)\simeq\frac{2q\cosh(\kappa_D a)}{4\pi\epsilon}\frac{\exp(-\kappa_D r)}{r}.$$

There is consequently a residual anistropy factor [here $\cosh(\kappa_D a)$] between the two directions, which does not disappear at large distances r from the charges (Fig. 1).

The same result is expected to hold for anisotropic macromolecules, with a residual and potentially strong anisotropy at large distances. The corresponding generalization of the DLVO theory is thus required. We emphasize immediately that the proposed description is mostly relevant in the case of moderately disymmetric objects, i.e., not too large aspect ratio, since the interaction energy we shall compute is valid for distances between the objects larger than their typical size (this precludes infinite objects). This is anyway the case for many macromolecules (Laponite clays, Boehmite rods, etc.).

The purpose of the present paper is twofold.

(1) We shall first describe in a general way the far field interaction between two anisotropic macromolecules. This will lead to a generalized DLVO interaction between two nonspherical molecules, with a formal expression of the anisotropic interaction factor.

(2) We shall then apply these results to the case of finite cylinders. A by-product of this part of the work is the charge carried by the finite cylinder and a description of the edge effects on the cylinders. An approximate analytical model is proposed yielding results in good agreement with numerical calculations. Note that we chose the finite cylinder geometry, not only for its relevance for polyelectrolytes, but also because we expect edge effects to be particularly marked. This geometry is therefore a ''benchmark'' for the study of anisotropic electrostatic interactions.

As in the original calculation of Verwey and Overbeek,[1] the macromolecules are specified by a constant electrostatic potential on their surfaces and the electrostatic potential in the electrolyte solution is described at the level of the linearized mean-field Poisson–Boltzmann equation. However we will show extensively in a subsequent paper[19] that this assumption is justified for colloids bearing a large constant charge on their surfaces.[20] For small surface charges, the sketch of resolution presented thereafter can also be easily adapted.

This paper is organized as follows: We begin by presenting the general method we have developed to construct the solution of the problem. Then we deduce the general formula for the interaction between two anisotropic colloids at large distances. This yields a formal expression of the above-discussed anisotropic factors. We then apply this general method to the specific case of finite cylinders. We first obtain the charge distributions on the cylinder, exhibiting the so-called edge effects. The influence of electrolyte concentration and finite-size effects are discussed. An approximate analytical model is eventually proposed to describe these effects, yielding results in quantitative agreement with the numerical solution.

II. GENERAL CONSIDERATIONS AND DESCRIPTION OF THE PROBLEM

A. Method of resolution: The auxiliary surface charge

We consider a single charged macromolecule embeded in an infinite electrolyte solution. The solution is characterized by a Debye screening length, $\ell_D=1/\kappa_D$ and as emphasized earlier, we assume that the electrostatic potential at the surface of the macromolecule, Φ_0, is held constant.[1] The electrical double layer around the macromolecule is described at the level of the linearized Poisson–Boltzmann theory. This relies on a mean-field description of the microion clouds, together with a small potential assumption. An extensive discussion of all these assumptions can be found in

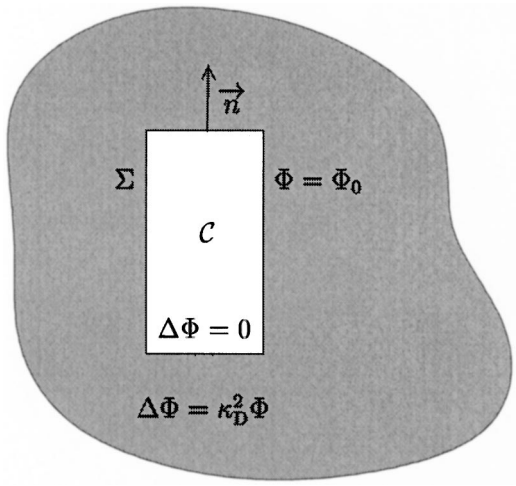

FIG. 2. Geometry of the problem. A macromolecule $\mathcal{C}$, with a surface potential $\Phi=\Phi_0$, is immersed in an infinite electrolyte. The permittivity of the macromolecule is assumed to be much lower than that of the solvent(water), so that the electrostatic potential is assumed to be constant in the interior of $\mathcal{C}$.

Refs. 1 and 20. We anticipate, however, that the assumption of a constant potential at the macromolecule boundary naturally emerges as an *effective condition* to describe correctly the far field obtained within the full nonlinear Poisson–Boltzmann theory, for colloids with a large bare charge, provided $\kappa_D a$ is not too small.[20,19]

In this context, outside the macromolecule, the electrostatic potential obeys the linearized Poisson–Boltzmann (LPB) equation,

$$\Delta\Phi(\mathbf{r})=\kappa_D^2\Phi(\mathbf{r}), \tag{2}$$

together with the boundary condition on the molecule surface Σ,

$$\Phi(\mathbf{r})=\Phi_0. \tag{3}$$

Note that we assume that the macromolecule interior is empty of charges, so that $\Phi(\mathbf{r})=\Phi_0$ for any point $\mathbf{r}$ inside the macroion [this amounts to writing $\Delta\Phi(\mathbf{r})=0$].

The surface charge density, σ, is then obtained from the derivative of the electrostatic potential at the molecule surface:

$$\sigma(\mathbf{r})=-\epsilon\left(\frac{\partial\Phi}{\partial\mathbf{n}}\right)_{\Sigma^+}, \tag{4}$$

where $\mathbf{n}$ is the (outer) unitary vector perpendicular to Σ and the notation $(\partial\Phi/\partial\mathbf{n})_{\Sigma^+}$ stands for $\mathbf{n}\cdot\nabla\Phi$ (Fig. 2).

The standard Green function formalism is too cumbersome to be applied in its simplest version to solve the previous equations—Eqs. (2) and (3). This is due to the existence of a nonvanishing excluded region for the microions (inside the macromolecule), where the LPB equation, Eq. (2), does not apply. In other words, the relevant Green's function for the problem depends on particular shape and size, which seriously limit its practical interest. To circumvent this difficulty, we have therefore introduced an auxilary system, in which the LPB equation applies everywhere in the volume. This is defined as

$$\begin{cases} \text{for } \mathbf{r}\in\mathcal{C} & \Delta\Phi(\mathbf{r})=\kappa_D^2\Phi(\mathbf{r}), \\ \text{for } \mathbf{r}\notin\mathcal{C} & \Delta\Phi(\mathbf{r})=\kappa_D^2\Phi(\mathbf{r}), \\ \text{for } \mathbf{r}\in\Sigma & \Phi(\mathbf{r})=\Phi_0. \end{cases} \tag{5}$$

The corresponding surface charge on the molecule, $\tilde{\sigma}$, is defined here in terms of the solution $\Phi_{\text{full}}(\mathbf{r})$ of the previous system of equations:

$$\tilde{\sigma}(\mathbf{r})=\epsilon\left[\left(\frac{\partial\Phi_{\text{full}}(\mathbf{r})}{\partial\mathbf{n}}\right)_{\Sigma^-}-\left(\frac{\partial\Phi_{\text{full}}(\mathbf{r})}{\partial\mathbf{n}}\right)_{\Sigma^+}\right]. \tag{6}$$

Of course, the solution of Eq. (5), $\Phi_{\text{full}}(\mathbf{r})$, reduces to the solution of Eq. (2), $\Phi_{\text{empty}}(\mathbf{r})$, outside the macromolecule. This matching originates in the unicity theorem for the operator $-\Delta+\kappa_D^2$ with Neumann or Dirichlet boundary conditions (see Ref. 18 for a similar result concerning the bare Laplace operator Δ).

Now, the solution of Eq. (5), $\Phi_{\text{full}}(\mathbf{r})$ can be defined in terms of the surface charge $\tilde{\sigma}$:

$$\Phi_{\text{full}}(\mathbf{r})=\int\int_{\Sigma}\tilde{\sigma}(\mathbf{r}')G(\mathbf{r},\mathbf{r}')dS', \tag{7}$$

where $G(\mathbf{r},\mathbf{r}')$ is the screened electrostatic Green function, $G(\mathbf{r},\mathbf{r}')=\exp(-\kappa_D|\mathbf{r}-\mathbf{r}'|)/(4\pi\epsilon|\mathbf{r}-\mathbf{r}'|)$. The unknown auxiliary charge, $\tilde{\sigma}$, is found by inverting the boundary condition on the macromolecule. This can be explicitly written as: for any point $\mathbf{r}$ on the molecule,

$$\Phi_0=\int\int_{\Sigma}\tilde{\sigma}(\mathbf{r}')G(\mathbf{r},\mathbf{r}')dS'. \tag{8}$$

The overall result of these general considerations is a formal solution of the LPB equation, Eq. (2), for any point outside the macromolecule:

$$\Phi(\mathbf{r})=\epsilon\int\int_{\Sigma}\tilde{\sigma}(\mathbf{r}')G(\mathbf{r},\mathbf{r}')dS' \tag{9}$$

with the auxiliary charge $\tilde{\sigma}$ defined in Eq. (8).

To get back to the "real" charge on the macromolecule, one has to compute the surface charge density as a function of the auxiliary quantity, $\tilde{\sigma}$. Using the definition

$$\sigma(\mathbf{r})=-\epsilon\left(\frac{\partial\Phi(\mathbf{r})}{\partial\mathbf{n}}\right)_{\Sigma^+}$$

on any point $\mathbf{r}$ on the colloid surface Σ, one obtains:

$$\sigma(\mathbf{r})=\int\int_{\Sigma}\tilde{\sigma}(\mathbf{r}')\left[-\frac{\partial[G(\mathbf{r}',\mathbf{r})]}{\partial\mathbf{n}}\right]_{\Sigma^+}dS'. \tag{10}$$

In practice, the calculation of $\tilde{\sigma}$ which requires the inversion of the boundary condition, Eq. (8), can be performed analytically for simple geometries only, spheres or infinite rods (see the following). For a more complex case, such as finite cylinders as considered in this paper, a numerical calculation has to be performed to compute the inverse matrix of $G(\mathbf{r},\mathbf{r}')$ on the (discretized) macroion. We shall show, however, that a simple model can be proposed which yields results in quantitative agreement with the numerical calculation.

In the case of a given surface charge $\sigma(\mathbf{r})$, this method of resolution can also be used to calculate the electrostatic potential $\Phi(\mathbf{r})$ outside the colloid by computing the auxiliary charge $\tilde{\sigma}(\mathbf{r}')$ at any point $\mathbf{r}'$ of Σ using Eq. (10) and then applying Eq. (9). Once again, the auxiliary charge $\tilde{\sigma}$ is the most relevant parameter to deal with the electrostatic potential created by a colloid immersed in an ionic fluid.

B. The spherical case as an illustrative example

Before going further, we come back to the simple spherical problem, where all previous different quantities, such as the bare and auxiliary surface charge, can be explicitly computed either by solving the LPB equation straightforwardly, or by using the above-sketched auxiliary charge method.

We consider an empty sphere Σ of radius a, at a constant surface potentiel Φ_0. On the one hand, the solution of the LPB equation is the usual Yukawa potential:

$$\Phi(r)=\Phi_0 a\,\frac{e^{-\kappa_D(r-a)}}{r}. \tag{11}$$

The surface charge σ is defined as

$$\sigma=-\epsilon\frac{d\Phi}{dr}(r=a)$$

and is therefore given by

$$\sigma=\epsilon\kappa_D\left(1+\frac{1}{\kappa_D a}\right)\Phi_0. \tag{12}$$

On the other hand, the above-described auxiliary problem consists in a sphere $\mathcal{S}$ filled with the electrolyte. Using the screened electrostatic Green function $G(\mathbf{r},\mathbf{r}')=\exp(-\kappa_D|\mathbf{r}-\mathbf{r}'|)/(4\pi\epsilon|\mathbf{r}-\mathbf{r}'|)$, one may invert the integral equation, Eq. (8), to obtain the (uniform) auxiliary charge:

$$\tilde{\sigma}=\epsilon\kappa_D[1+\coth(\kappa_D a)]\Phi_0. \tag{13}$$

It is then straightforward to show that performing the integral in Eq. (10) allows one to recover the above-obtained surface charge density, Eq. (12).

This simple example illustrates the difference between the bare and auxiliary problems which we have introduced in the previous section and two ways to calculate the real charge σ as a function of Φ_0. The first method could only be used because we knew the formal solution of LPB for a sphere at fixed potential but this is an exception rather than the rule. On the contrary, the auxiliary charge method, even if it seems less straightforward in this case, is a systematic way to compute the solution of LPB for given boundary conditions.

We now turn to the calculation of the interaction energy between two macromolecules.

III. FAR-FIELD INTERACTION BETWEEN ANISOTROPIC HIGHLY CHARGED COLLOIDS

Before focusing on a specific geometry, we first use the previous results to describe the interaction between two anisotropic charged macromolecules.

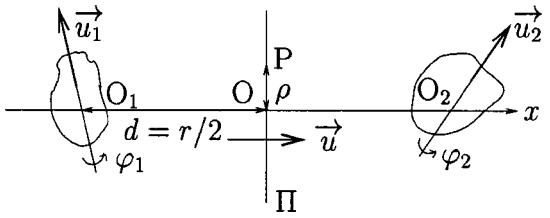

FIG. 3. Calculation of the electrostatic interaction between two disymmetric macromolecules. An arbitrary center O_i, a unit vector $\mathbf{u}_i$, and a rotation angle φ_i are defined for each molecule. We denote as $r=|O_1O_2|$ the distance between the two molecules, while the unit vector $\mathbf{u}$ is defined as $\mathbf{u}=\mathbf{O_1O_2}/|O_1O_2|$. We eventually introduce the bisector plane Π and the intersection point O between Π and O_1O_2.

We consider two colloids $\mathcal{C}_i$ $(i=1,2)$ separated by a distance r much larger than the typical size D of the colloids. As we already noticed in Sec. I, it is important to note that the restriction $r\geqslant D$ makes sense for moderately disymmetric macromolecules only. We assume at this level that the charge profiles $\sigma_i(\mathbf{r})$, and equivalently $\tilde{\sigma}_i(\mathbf{r})$, are known. The position of each colloid $\mathcal{C}_i$ is characterized by fixing a (somewhat arbitrary) origin O_i for the molecule (this may coincide for example with the colloid center if it is symmetrical). On the other hand, we assume that the orientation of the anisotropic colloid is described by a unit vector $\mathbf{u}_i$ pointing into a direction Ω_i and an angle φ_i corresponding to a rotation of $\mathcal{C}$ around $\mathbf{u}_i$. We finally define the colloid–colloid direction using the unit vector $\mathbf{u}=\mathbf{O_1O_2}/|O_1O_2|$ and introduce the bisector plane, Π, of $[O_1O_2]$ and O the intersection of Π with (O_1O_2). It will prove useful to introduce of system of coordinates $\{O,x,y,z\}$, with the x axis corresponding to the axis (O_1O_2) (see Fig. 3). The distance between O and a point P is denoted as ρ.

We shall estimate the interaction force (acting on one macromolecule due to the other) by integrating the electrostatic stress tensor, $\vec{\vec{T}}$, defined as[18]

$$\vec{\vec{T}}=\left(P+\frac{\epsilon\mathbf{E}^2}{2}\right)\vec{\vec{I}}-\epsilon\mathbf{E}\otimes\mathbf{E}, \tag{14}$$

where $\vec{\vec{I}}$ is the identity tensor, $\mathbf{E}$ the electrostatic field, and P the hydrostatic pressure.

The force acting on the macromolecule $\mathcal{C}_2$ can be written accordingly as

$$\mathbf{F}_2=-\int\int_{\Pi}\vec{\vec{T}}\,d\mathbf{S}. \tag{15}$$

Note that the integral runs over the bisector surface Π, and not the colloid surface. This is a consequence of the fact that the divergence of the eletrostatic stress tensor $\vec{\vec{T}}$ vanishes outside the macroions.

We emphasize that the following calculations are conducted in the far field limit where the distance r is larger than the Debye length $\ell_D=\kappa_D^{-1}$. This will allow us to expand the various quantities in powers of ρ/r. No specific assumption is done however on the ratio between the typical size of the macromolecule, a, and ℓ_D.

Hydrostatic equilibrium and (linearized) Poisson–Boltzmann equations, respectively, $-\mathbf{grad}\,p+\rho\mathbf{E}=\mathbf{0}$ and $\Delta\Phi=\kappa_D^2\Phi$, allow us to write $P=P_\infty+\epsilon\kappa_D^2\Phi^2/2$. Note that the linearization of the PB equation is fully justified in the present case since in the far field limit ($r\gg\kappa_D^{-1}$) the dimensionless electrostatic potential $e\Phi/k_BT$ is expected to be small. One therefore obtains

$$\vec{\vec{T}}=\left(P_\infty+\tfrac{1}{2}\epsilon\kappa_D^2\Phi^2-\frac{\epsilon}{2}\mathbf{E}^2\right)\vec{\vec{I}}-\epsilon(\mathbf{E}\otimes\mathbf{E}-\mathbf{E}^2)\vec{\vec{I}}. \tag{16}$$

We denote E_α the component of $\mathbf{E}$ in the direction α, $\alpha=x,\,y,\,z$. Then, for $P\in\Pi$:E_y, $E_z=\mathcal{O}(\rho/r)E_x$. Therefore, $\mathbf{E}^2=E_x^2[1+\mathcal{O}(\rho^2/r^2)]$ and $E_\alpha E_\beta-E_\alpha^2\delta_{\alpha\beta}=E_x^2+\mathcal{O}(\rho^2/r^2)$.

This allows one to rewrite the force $\mathbf{F}_2$ acting on colloid 2 as

$$\mathbf{F}_2\simeq\left\{\int\int_\Pi\frac{\epsilon}{2}[\kappa_D^2\Phi^2(\rho)-E_x^2(\rho)]\right\}d\mathbf{S}. \tag{17}$$

Both the potential Φ and the electric field E_x in Eq. (17) can be estimated from the solution for the potential created by a single colloid, as obtained in the previous paragraph, as we now show. First Eq. (9) can be written

$$\Phi(\mathbf{r})=\int\int_\Sigma\tilde{\sigma}(\mathbf{r}')\frac{\exp(-\kappa_D|\mathbf{r}-\mathbf{r}'|)}{4\pi\epsilon|\mathbf{r}-\mathbf{r}'|}dS'. \tag{18}$$

For distances r much larger than the typical size a of the macromolecule $\mathcal{C}_i$, one might expand the previous equation for small r' to obtain the leading large r contribution:

$$\Phi(\mathbf{r})=\frac{\exp(-\kappa_D r)}{4\pi\epsilon r}\int\int_\Sigma\tilde{\sigma}(\mathbf{r}')\exp(-\kappa_D\mathbf{u}_r\cdot\mathbf{r}')dS', \tag{19}$$

with $\mathbf{u}_r=\mathbf{r}/r$. We introduce at this point the total auxialiary charge $\tilde{Z}_i=\int_{\Sigma_i}\tilde{\sigma}(\mathbf{r}')dS'$ and the angular distribution $f_i(P)$ defined as

$$f_i(P)=1/\tilde{Z}_i\int\int_\Sigma\tilde{\sigma}(\mathbf{r}')\exp(-\kappa_D\mathbf{u}_r\cdot\mathbf{r}')dS'. \tag{20}$$

Using these definitions, one gets eventually the electrostatic potential at point P as

$$\Phi_i(P)=\frac{\tilde{Z}_i f_i(P)e^{-\kappa_D r}}{4\pi\epsilon r}. \tag{21}$$

At the order $\mathcal{O}(\rho/r)$, it is straightforward to check that one might replace $\mathbf{u}_r$ by $\mathbf{u}$ in the anisotropic factor f_i of the previous equation: f_i only depends on the angular coordinates (characterized by $\mathbf{u}_i$ and φ_i). Note that the dependence on φ_i disappears for axisymmetric colloids. From now on, we will only consider such objects so that may write $f_i=f_i(\mathbf{u}_i)$ for simplification. The potential created by colloid i therefore reads

$$\Phi_i(P)=\frac{\tilde{Z}_i f_i(\mathbf{u}_i)e^{-\kappa_D r}}{4\pi\epsilon r}. \tag{22}$$

In the $r\gg\kappa_D^{-1}$ limit, the corresponding electric field reduces to $\mathbf{E}_i=\pm\kappa_D\Phi_i(P)\mathbf{u}$, with a plus (respectively, minus) sign for $i=1$ (respectively, $i=2$). The total electrostatic potential Φ on the mediator plane Π is written as the sum of the contributions due to each colloid, $\Phi=\Phi_1+\Phi_2$:

$$\Phi(P)=(\tilde{Z}_1 f_1(\mathbf{u}_1)+\tilde{Z}_2 f_2(\mathbf{u}_2))\frac{e^{-\kappa_D r}}{4\pi\epsilon r}. \tag{23}$$

Note that the superposition assumption for the potential is justified in the far field limit, where one may neglect mutual polarization effects. The same holds for the electric field: $E_x=E_1+E_2$, leading to

$$E_x=\kappa_D(\tilde{Z}_1 f_1(\mathbf{u}_1)-\tilde{Z}_2 f_2(\mathbf{u}_2))\frac{e^{-\kappa_D r}}{4\pi\epsilon r}\mathbf{u}. \tag{24}$$

Introducing these expressions into Eq. (17) yields the following expression for the force $\mathbf{F}_2$:

$$\mathbf{F}_2=\frac{2\kappa_D^2\tilde{Z}_1\tilde{Z}_2 f_1(\mathbf{u}_1)f_2(\mathbf{u}_2)}{(4\pi)^2\epsilon}\times\int_0^\infty 2\pi\rho\,d\rho\,\frac{e^{-2\kappa_D\sqrt{d^2+\rho^2}}}{d^2+\rho^2}\mathbf{u}. \tag{25}$$

In the far field region, $r\gg\kappa_D^{-1}$, it is legitimate to expand the integrand in powers of ρ/r and keep only the leading order: using $e^{-2\kappa_D\sqrt{d^2+\rho^2}}=e^{-\kappa_D r(1+4\rho^2/r^2+\mathcal{O}(\rho^4/r^4))}$, one may compute the integral to get

$$\mathbf{F}_2=\frac{\tilde{Z}_1\tilde{Z}_2 f_1(\mathbf{u}_1)f_2(\mathbf{u}_2)e^{-\kappa_D r}}{4\pi\epsilon r}\kappa_D\mathbf{u}, \tag{26}$$

which is always repulsive.[21] This force derives form the potential energy (again at leading order in $\kappa_D r$):

$$U_{12}(r)=\frac{\tilde{Z}_1\tilde{Z}_2 f_1(\mathbf{u}_1)f_2(\mathbf{u}_2)e^{-\kappa_D r}}{4\pi\epsilon r}. \tag{27}$$

This expression for the interaction energy between the two macromolecules is one of the main results of this paper. This generalizes the DLVO calculation for anisotropic molecules. Note that, in view of the various expansions performed, this expression is valid in the far-field limit, i.e., for interparticle distances r larger than both the Debye length and the typical size of the colloid a (say, to fix the ideas, $r>4\ell_D,\,4a$).

As anticipated in Sec. I, the interaction does not reduce at any distance to the isotropic DLVO result, obtained for spheres. The anisotropy of the interaction is described by the angular distribution $f_1(\mathbf{u}_1)$ and $f_2(\mathbf{u}_2)$ defined in Eq. (20). The latter is defined in terms of the (auxiliary) charge distribution on the macromolecules $\tilde{\sigma}(\mathbf{r})$, or equivalently as a function of the bare surface charge $\sigma(\mathbf{r})$ using Eq. (10).

We conclude this part by showing that the previous expression for the interaction energy indeed reduces to the standard DLVO expression for spheres (as it should). In this case, the bare and auxiliary surface charges on one sphere have-been computed in the previous section, in Eqs. (12) and (13). On the other hand, the angular factor f_i for each sphere i can be easily computed and reduces to $f_i=\sinh\kappa_D a/\kappa_D a$. The latter is of course independent of any angular variable. Gathering these results, one retrieves the DLVO expression, Eq. (1):

$$U_{12}=\left(\frac{e^{\kappa_D a}}{1+\kappa_D a}\right)^2 \frac{Z_1 Z_2 e^{-\kappa_D r}}{4\pi\epsilon r}. \tag{28}$$

A final note concerns the case of colloids with vanishing internal volumes. In the latter case, the bare and auxiliary charge coincide, $\tilde{\sigma}=\sigma$, and our calculation leads back to the expression found in a different context by Trizac *et al.*:[17]

$$U_{12}=\frac{Z_1 Z_2 e^{-\kappa_D r}}{4\pi\epsilon r} f_1(\mathbf{u}_1) f_2(\mathbf{u}_2). \tag{29}$$

IV. CHARGE DISTRIBUTION ON A FINITE ROD-LIKE POLYELECTROLYTE

We now use the previous results to predict the far field interaction between two finite rod-like polyelectrolytes. In contrast to the spherical case, briefly considered in Sec. III, the surface charge cannot be obtained analytically in this situation. Therefore, we shall first obtain numerically the surface charge on the cylinder, by solving Eq. (8). We will then propose a simple analytical model yielding an approximate surface charge in good agreement with the ''exact'' numerical results.

We emphasize at this point that the finite cylinder geometry should be merely considered here as a generic situation where end effects are important. The present description could be easily extended to other related geometries, like sphero-cylinders, ellipsoids, etc., though no fundamental difference is however expected.

A. Sketch of the numerical method

We now consider a cylinder $\mathcal{C}$ with radius R and length L, at a contant potential Φ_0. The resolution first starts with the computation of the auxiliary surface charge by inverting Eq. (8). This calculation involves the Green function $G(\mathbf{r},\mathbf{r}')$, $G(\mathbf{r},\mathbf{r}')=\exp(-\kappa_D|\mathbf{r}-\mathbf{r}'|)/(4\pi\epsilon|\mathbf{r}-\mathbf{r}'|)$, expressing the potential at point $\mathbf{r}'$ created by a unit point charge in $\mathbf{r}$. However due to the cylindrical symmetry of the problem, one might reduce the dimensionality of the problem by integrating the Green function on a ring (or small cylinder) whose center matches the axis of symmetry of the cylinder, as illustrated in Fig. 4. This specific problem is considered in the following. Once the corresponding reduced Green function is known, the numerical task simplifies into a standard inversion problem. First, the cylinder $\mathcal{C}$ is decomposed into the superposition of small cylinders (on the lateral surface) or rings (on the head surfaces), denoted as $\mathcal{C}_j$ and $\mathcal{R}_k$, with dimension ℓ and surface charge density $\tilde{\sigma}_i$ (see Fig. 4).

Then Eq. (8) is discretized according to

$$\forall j\in\Sigma, \Phi(\mathbf{r}_j)=\sum_i \tilde{\sigma}_i G_i(\mathbf{r}_i,\mathbf{r}_j)=\Phi_0, \tag{30}$$

where $G_i(\mathbf{r}_i,\mathbf{r}_j)$ is the electrostatic potential created on the cylinder $\mathcal{C}_j$ or ring $\mathcal{R}_j$ by the cylinder $\mathcal{C}_i$ or ring $\mathcal{R}_i$, carrying a unit surface charge density.

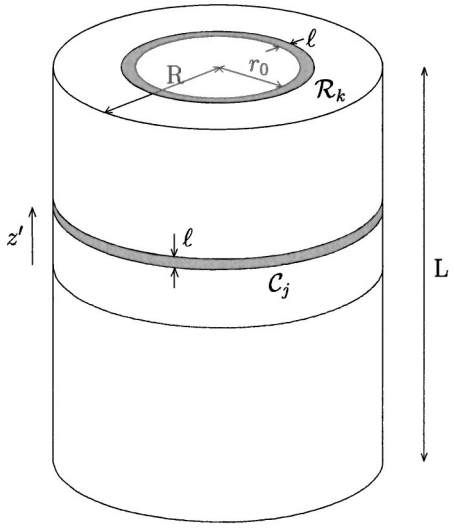

FIG. 4. The numerical calculations are performed by decomposing the cylinder $\mathcal{C}$ into small cylinders $\mathcal{C}_j$ of radius R and height ℓ, and in rings $\mathcal{R}_k$ of radii r_0 and of width ℓ. Each of these elementary surfaces carry a uniform surface charge density $\tilde{\sigma}_i$. The numerical calculations were performed with $\ell\leqslant 0.05\ell_D$.

B. Reduced Green function

As mentioned earlier, the previous inversion requires knowledge of the potential created by an elementary ring or cylinder, which we now compute. To this end, we make use of the explicit expression of the electrostatic potential created by a disk of radius R at heigh z' carrying a uniform surface charge density (here equal to unity) and immersed in an electrolyte with Debye length ℓ_D. This expression can be found in Ref. 22 and reads:

$$G_{\text{disk}}(R,r,z)=\frac{R}{2\epsilon}\int_0^\infty \frac{J_1(kR)J_0(kr)}{\sqrt{k^2+\kappa_D^2}} \times\exp(-\sqrt{k^2+\kappa_D^2}|z-z'|)dk \tag{31}$$

with J_0 and J_1 the Bessel functions of order 0 and 1. This is namely the potential created by a *disk* with radius R at a point M, with cylindrical coordinates $\{r,z\}$ (the origin being placed at the center of the disk). Note also that the dimension of G_{disk} is given by R/ϵ, since G_{disk} is the potential created by a unit surface charge.

Now the potential $dG_{\text{cyl}}(R,r,z)$ created, at a point M, by an infinitesimal *cylinder* with height dz', radius R, and unit surface charge can be deduced directly as

$$dG_{\text{cyl}}(R,r,z)=dz'\frac{\partial G_{\text{disk}}(R,r,z)}{\partial R}. \tag{32}$$

This leads to

$$dG_{\text{cyl}}(R,r,z)=\frac{Rdz'}{2\epsilon}\int_0^\infty \frac{kJ_0(kr)J_0(kR)}{\sqrt{k^2+\kappa_D^2}} \times\exp(-\sqrt{k^2+\kappa_D^2}|z-z'|)dk, \tag{33}$$

where the identity $(d/dx)[xJ_1(x)]=xJ_0(x)$ has been used.

As a result, the electrostatic potential created by a cylinder of radius R, height ℓ, and unit surface charge, with a center located in $(0,z')$, is given by

$$G_{\rm cyl}(R,z',r,z)=\frac{R}{2\epsilon}\int_{z'-\ell/2}^{z'+\ell/2}dz''\int_0^\infty \frac{kJ_0(kr)J_0(kR)}{\sqrt{k^2+\kappa_D^2}} \times\exp(-\sqrt{k^2+\kappa_D^2}|z-z''|)dk. \quad (34)$$

Along the same lines, the potential $G_{\rm ring}(r_0,r,z)$ created by the ring of radius r_0 and of thickness ℓ can be expressed in terms of $G_{\rm disk}(r_0,r,z)$ according to

$$G_{\rm ring}(r_0,r,z)=G_{\rm disk}(r_0+\ell/2,r,z)-G_{\rm disk}(r_0-\ell/2,r,z), \quad (35)$$

where $G_{\rm disk}(R,r,z)$ is given above in Eq. (31).

Note that in order to avoid numerical problems, the previous integrals must be reformulated specifically for the case $z=z'$.

C. Calculation of the surface charge

Inversion of Eq. (30) yields the auxiliary surface charge $\tilde{\sigma}$. The "real" surface charge, σ, can be deduced from $\tilde{\sigma}$ using Eq. (10). In a discretized form, this reads

$$\forall j\in\Sigma,\sigma(\mathbf{r}_j)=-\sum_i \tilde{\sigma}_i\frac{\partial G_i(\mathbf{r}_i,\mathbf{r}_j)}{\partial \mathbf{n}_j}, \quad (36)$$

where G_i takes either the cylinder or the ring form, obtained in Eqs. (34) and (35). This equation involves various derivatives of the Green function at the cylinder surface, namely,

$$\left(\frac{\partial G_{\rm cyl}}{\partial r}\right)_{r=R^+},\quad \left(\frac{\partial G_{\rm cyl}}{\partial z}\right),\quad \left(\frac{\partial G_{\rm disk}}{\partial r}\right)_{r=R^+},\quad \left(\frac{\partial G_{\rm disk}}{\partial z}\right).$$

It will turn out to be useful to write all the results in terms of dimensionless variables. All the lengths (such as ℓ_B, κ_D^{-1}, or L) are expressed in units of the radius of the cylinder R, e.g., $L^{\rm adim}=L/R$. In the same way, the electrostatic potential Φ and surface charge densities σ become, respectively, $\Phi^{\rm adim}=e\Phi/k_BT$ and $\sigma^{\rm adim}=4\pi\ell_BR\sigma/e$ where we recall that ℓ_B is the Bjerrum length defined by $\ell_B=e^2/(4\pi\epsilon k_BT)$ (for water at room temperature, $\ell_B=7$ Å). We also introduce dimensionless Green functions, as $G^{\rm adim}=\epsilon G/R$ (see the previous remark on the dimension of G). From now on, the index "adim" will be omitted to simplify notations.

D. Numerical results

The previous equations are easily implemented numerically, provided the various expressions of the Green functions are written in terms of well-converging integrals as mentioned earlier.

To fix ideas the potential on the macromolecule is assumed to be $V_0\simeq 100$ mV, so that $\Phi_0=4$ (see however Refs. 20 and 19 for further justifications of this choice).

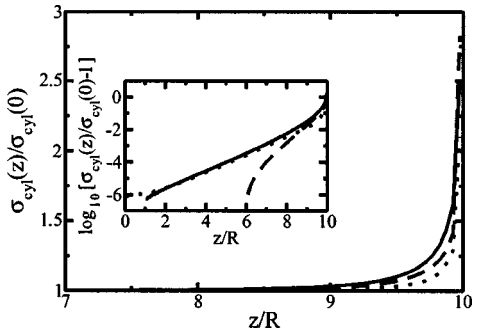

FIG. 5. Plot of the reduced surface charge on the lateral side of the cylinder, $\ln[\sigma_{\rm cyl}(z/R)/\sigma_{\rm cyl}(0)-1]$. The aspect ratio of the cylinder is $L/R=20$ and the screening factor is $\kappa_DR=1.0$. Note that z is in units of the cylinder radius R. The solid line is the result of the full numerical calculations, while the dashed line is the result of the "four parameter" model described in the Appendix. The dotted line is the (reduced) auxiliary surface charge $\tilde{\sigma}_{\rm cyl}(z/R)/\tilde{\sigma}_{\rm cyl}(0)$. Note that the edge effect spans over a smaller distance for the auxiliary surface charge, compared to the "real" charge. See the text for details.

1. Surface charge profiles

We now present the results for the surface charges on the lateral and the head of the cylinder, that we shall denote, respectively, as $\sigma_{\rm cyl}(z)$ and $\sigma_{\rm head}(z)$. We first focus on the shape of the profiles.

Typical results for these profiles are shown in Figs. 5 and 6.

Qualitatively, the main striking feature of these profiles is the diverging surface charge close to the edges of the cylinder. This is of course the well-known edge effect, which is expected for charged objects with uniform potential. In the absence of electrolyte ($\kappa_D=0$), the divergence of the surface charge in the vicinity of an edge is a classical result.[18] For an infinite conducting diedre with an edge angle β, the surface charge density σ is found to diverge in the vicinity of the edge as $\rho^{\pi/\beta-1}$, where ρ is the distance to the edge.[18] In the present geometry, corresponding to $\beta=3\pi/2$, the surface charge is expected to diverge as $\rho^{-1/3}$. For a charged object embedded in an electrolyte, i.e., $\kappa_D\neq 0$, the situation is more complex. However the divergence is expected to remain, as can be understood from a simple argument. As mentioned

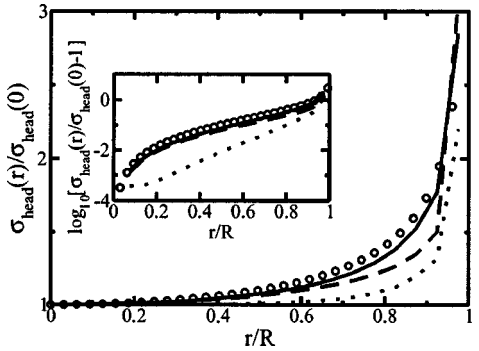

FIG. 6. Same as Fig. 5, but for the surface charge profile on the head of the cylinder $\ln[\sigma_{\rm head}(z/R)/\sigma_{\rm head}(0)-1]$. We have also plotted the predicted scaling for the divergence in the absence of salt $\kappa_DR=0$, $\sigma_{\rm head}(z/R)/\sigma_{\rm head}(0)=(1-(r/R)^2)^{-1/3}$ (open circles).

in Sec. II B, the surface charge on a sphere with radius a and constant potential Φ_0 reads

$$\sigma = \epsilon\kappa_D\left(1+\frac{1}{\kappa_D a}\right)\Phi_0$$

[see Eq. (12)]. Now using this relationship for a nonspherical object, one finds that the surface charge σ diverges at the points where the radius of curvature a vanishes.

Figures 5 and 6 show that the auxiliary surface charge $\tilde{\sigma}$ also exhibits an edge effect. However the latter is more localized close to the edge, compared to the ''real'' surface charge σ. As for σ, the divergence of $\tilde{\sigma}$ can be understood using the results for the sphere, $\tilde{\sigma}=\epsilon\kappa_D[1+\coth(\kappa_D a)]\Phi_0$, which indeed diverges as the radius of curvature a vanishes. However, the transition from a small a region to a large a region is much more marked for the auxiliary surface charge than for the bare charge. Indeed from the previous expressions for σ and $\tilde{\sigma}$, one gets $\sigma(a)=\sigma(a=\infty)+\mathcal{O}(1/\kappa_D a)$, while $\tilde{\sigma}(a)=\tilde{\sigma}(a=\infty)+\mathcal{O}(\exp[-\kappa_D a])$. The large a limit is therefore approached much more quickly for the auxiliary charge than for the bare charge, which is in agreement with the stronger localization of the divergence of the auxiliary charge close to the edge.

We now report in more detail on the variations of these density profiles when the size of the cylinder L and the screening length κ_D^{-1} are varied. Generally speaking, the geometry of the problem is characterized by two dimensionless quantities: the aspect ratio L/R and the amounts of screening $\kappa_D R$. Some general trends for the surface charge profiles emerge when these quantities are varied. First, the lateral surface profiles are found to saturate as the aspect ratio L/R goes to infinity. On the other hand, the head profile is found to be barely dependent on the aspect ratio. One expects in fact that the cylinder length L will only play a role when it is smaller or equal to the Debye length, κ_D^{-1}, say $\kappa_D L \leqslant \alpha$, with α of the order of a few units to fix ideas. Therefore for a given screening $\kappa_D R$, the profile is expected to saturate for aspect ratio larger than $L/R \sim \alpha/(\kappa_D R)$. This rule of thumb is confirmed when $\kappa_D R$ is varied. In the present study, we have verified this assertion in the interval $\kappa_D R \in [0.1;1]$ (data not shown). Typically one finds $\alpha \sim 5$. Finally it is interesting to compare both profiles with the edge effect divergence predicted in the $\kappa_D=0$ limit, as argued earlier. Only the charge profile on the head is found to be in semiquantitative agreement with this scaling, as shown in Fig. 6. Note that in order to symmetrize the predicted divergence, we compare the head profile with $\sigma_{\text{head}}(r)/\sigma_{\text{head}}(0)=(1-(r/R)^2)^{-1/3}$. On the other hand this prediction is found to fail for the cylinder surface charge. This is expected since in most of the present calculations, the length L of the cylinder is larger than the Debye length, so that the $\kappa_D=0$ profile is only a very crude approximation. On the other hand, the radius of the cylinder is always smaller than the Debye length considered, and for the head, the $\kappa_D=0$ profile should be a fair but not so bad approximation for $\kappa_D R \leqslant 1$.

2. Total lateral and head charge

A more global quantity of interest is the total charge on the lateral surfaces and on each head of the cylinder, respectively denoted as $Z_{\text{lat}}e$ and $Z_{\text{head}}e$ (e being the elementary charge). It proves in fact useful to consider the average surface charges on the lateral surface $\sigma_{\text{lat}}^{\text{average}}=Z_{\text{lat}}/(2\pi RL)$ and on each head of the cylinder, $\sigma_{\text{head}}^{\text{average}}=Z_{\text{head}}/(\pi R^2)$ (note that in the following we plot the above-introduced *reduced* surface charge densities as $\sigma^*=4\pi\ell_B R\sigma/e$). These quantities are plotted, respectively, in Figs. 7 and 8 as a function of the length of the cylinder L/R for various screenings $\kappa_D R$. In the limit of large aspect ratio, both charges saturate to finite values. Moreover, both charges are found to be increasing functions of the screening $\kappa_D R$. This is expected, as can be understood from the spherical test case, Eq. (12), as a benchmark.

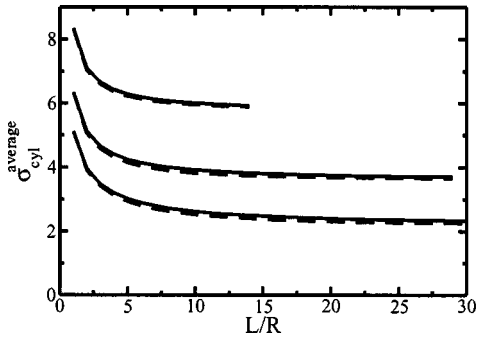

FIG. 7. Dependence of the averaged surface charge on the cylinder, $\sigma_{\text{cyl}}^{\text{average}}$, as a function of the aspect ratio L/R. The solid line is the result of the full numerical calculation, while the dashed line corresponds to the four parameter model described in the Appendix. From bottom to top, the screening factors are $\kappa_D R=0.2$, $\kappa_D R=0.5$, and $\kappa_D R=1.0$. The $L=\infty$ asymptotic values are in agreement with the analytic result, Eq. (42).

V. ANALYTICAL DESCRIPTION OF THE SURFACE CHARGE

In this section, we propose a very simplified description of the electrostatic problem, which has the virtue of providing analytic estimates of the surface charges. This estimate will prove usefull *in fine* to compute the interaction between two rod-like polyelectrolytes. A more detailed approach, including a description of the edge effect, is proposed in the Appendix.

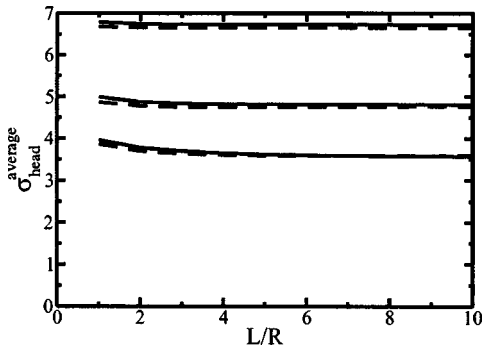

FIG. 8. Same as Fig. 7, but with the charge on the head of the cylinder, $\sigma_{\text{head}}^{\text{average}}$.

A. Uniform head and lateral surface charges

We consider a ''zeroth-order'' approximation of the problem, consisting in a cylinder with uniform charges on the head and on the lateral sides. More specifically, we assume a uniform *auxiliary* charge profile. We denote $\tilde{\sigma}_{\mathrm{cyl}}$ and $\tilde{\sigma}_{\mathrm{head}}$ the auxiliary surface charge on the cylinder and on the head, and by σ_{cyl} and σ_{head} the corresponding ''real'' surface charges.

At this level of approximation, Eq. (30) relating the *auxiliary surface* charge to the potential Φ_0 reduces to a 2×2 problem:

$$\begin{aligned}\Phi_0&=\tilde{\sigma}_{\mathrm{cyl}}G_{\mathrm{cyl}}(R,R,0)+2\tilde{\sigma}_{\mathrm{head}}G_{\mathrm{head}}(R,R,L/2),\\ \Phi_0&=\tilde{\sigma}_{\mathrm{cyl}}G_{\mathrm{cyl}}(R,0,L/2)+\tilde{\sigma}_{\mathrm{head}}[G_{\mathrm{head}}(R,0,0)\\ &\quad+G_{\mathrm{head}}(R,0,L)].\end{aligned}\tag{37}$$

The surface charges on the head and on the lateral side of the cylinder are then obtained using Eq. (10) as

$$\begin{aligned}\sigma_{\mathrm{cyl}}&=\tilde{\sigma}_{\mathrm{cyl}}\left(-\frac{\partial G_{\mathrm{cyl}}(R,r,0)}{\partial r}\right)_{R^+}+\tilde{\sigma}_{\mathrm{head}}\\ &\quad\left(-\frac{\partial G_{\mathrm{head}}(R,r,L/2)}{\partial r}\right)_{R^+},\\ \sigma_{\mathrm{head}}&=\tilde{\sigma}_{\mathrm{cyl}}\left(-\frac{\partial G_{\mathrm{cyl}}(R,0,z)}{\partial z}\right)_{L/2^+}+\tilde{\sigma}_{\mathrm{head}}\\ &\quad\left(-\frac{\partial G_{\mathrm{head}}(R,r,z)}{\partial z}\right)_{0^+}.\end{aligned}\tag{38}$$

In the previous equations, the derivatives of the Green functions are expressed in terms of integrals of Bessel functions [see Eqs. (31) and (34)], which have to be computed numerically for any L and κ. The systems in Eqs. (37) and (38) can be easily inverted to obtain the expressions of σ_{cyl} and σ_{head} as a function of the aspect ratio L/R and screening $\kappa_D R$.

Here we do not report the full expressions. Rather we consider the asymptotic $L\to\infty$ limit, in which the surface charges reach finite values. Note that this limit is reached for sizes L larger than a few Debye lengths.

In the infinite L limit, the various Green function may be computed, yielding

$$\begin{aligned}&G_{\mathrm{cyl}}(R,R,0)=I_0(\kappa_D R)K_0(\kappa_D R),\\ &G_{\mathrm{disk}}(R,R,L/2)=0,\\ &G_{\mathrm{cyl}}(R,0,L/2)=K_0(\kappa_D R)/2,\\ &G_{\mathrm{disk}}(R,0,0)=(1-e^{-\kappa_D R})/2\kappa_D R.\end{aligned}\tag{39}$$

In the same way,

$$\begin{aligned}&-(\partial/\partial r)G_{\mathrm{cyl}}(R,r=R^+,0)=\kappa_D R I_0(\kappa_D R)K_1(\kappa_D R),\\ &-(\partial/\partial z)G_{\mathrm{cyl}}(R,0,z=L/2^+)=\frac{e^{-\kappa_D R}}{2},\\ &-(\partial/\partial r)G_{\mathrm{disk}}(R,r=R^+,L/2)=0,\\ &-(\partial/\partial z)G_{\mathrm{disk}}(R,0,z=0^+)=\tfrac{1}{2}.\end{aligned}\tag{40}$$

Gathering results, we obtain after inversion of Eq. (37):

$$\begin{aligned}\tilde{\sigma}_{\mathrm{cyl}}^{\mathrm{uniform}}&=\frac{\Phi_0}{I_0(\kappa_D R)K_0(\kappa_D R)},\\ \tilde{\sigma}_{\mathrm{head}}^{\mathrm{uniform}}&=\frac{2\kappa_D R\Phi_0}{1-e^{-\kappa_D R}}\left[1-\frac{1}{2I_0(\kappa_D R)}\right].\end{aligned}\tag{41}$$

We now denote these profiles as ''uniform'' to avoid any confusion with the numerical results. Using Eq. (38), one gets the ''real'' surface charge densities:

$$\begin{aligned}\sigma_{\mathrm{cyl}}^{\mathrm{uniform}}&=\Phi_0\frac{\kappa_D R K_1(\kappa_D R)}{K_0(\kappa_D R)},\\ \sigma_{\mathrm{head}}^{\mathrm{uniform}}&=\frac{e^{-\kappa_D R}\Phi_0}{2I_0(\kappa_D R)K_0(\kappa_D R)}+\frac{\kappa_D R\Phi_0}{1-e^{-\kappa_D R}}\\ &\quad\times\left[1-\frac{1}{2I_0(\kappa_D R)}\right].\end{aligned}\tag{42}$$

In the limit of large $\kappa_D R$, the surface charges are linear in $\kappa_D R$. This is expected since in this limit, one retrieves the planar results for which $\sigma\propto\kappa\Phi_0$.

The previous result for $\sigma_{\mathrm{cyl}}^{\mathrm{uniform}}$ corresponds to the semi-infinite cylinder limit.[20] One may also verify in Fig. 7 that this result does indeed match the $L\to\infty$ limit of the averaged cylinder profile. Note that in contrast, one may verify that the uniform surface charge on the head $\sigma_{\mathrm{head}}^{\mathrm{uniform}}$ is only a fair approximation to the numerically computed averaged surface charge, even in the $L\to\infty$. This is because for the screening considered ($\kappa_D R\leqslant1$), the head always feels the edge of the cylinder.

B. Toward a description of the edge effect

A simple extension of the previous modelization can be proposed: adding a ''ring'' on the edge of the cylinder should allow one to capture the main features of the edge effect. This can be done in a straightforward way, but the details of the calculation are somewhat cumbersome. We therefore report the details of this approach in the Appendix. This ''four parameters'' model gives results in good agreement with the numerical solutions. This can be seen in Figs. 7 and 8, where the results of this model are displayed (as dashed lines) against the full numerical results.

However, the interactions between two polyelectrolytes do not involve the ''real'' charge, but the *auxiliary charge*. As we show in the following, the results of the much simpler ''uniform'' approach described in the previous paragraph will prove sufficient to describe the interaction between two rods.

VI. INTERACTION BETWEEN TWO ROD-LIKE POLYELECTROLYTES

We eventually turn to the description of the interaction between two rod-like polyelectrolytes. Our starting point is the potential energy obtained in Sec. III, Eq. (27). The two crucial ingredients in this interaction energy are: the total auxiliary charge $\tilde{Z}$ on the cylinder; and the anisotropic term, $f(P)$, defined in terms of the auxiliary charge profile in Eq. (20). We recall here this expression:

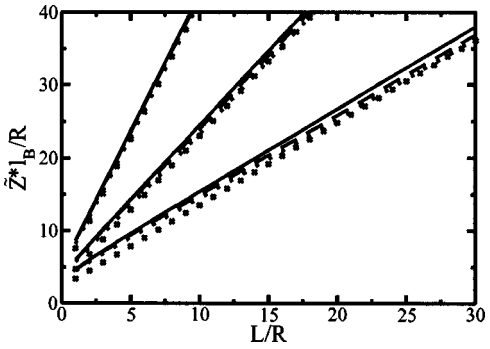

FIG. 9. Total auxiliary charge $\tilde{Z}_{\rm tot}\ell_B/R$ as a function of the size of the cylinder L/R. The solid line corresponds to the full numerical resolution, while the crosses are the result of the uniform model. The dashed line is the result of the four parameter model detailed in the Appendix. The dotted line corresponds to the uniform model with finite L (see the text for details). From bottom to top the screening factors are $\kappa_D R=0.2$, $\kappa_D R=0.5$, and $\kappa_D R=1.0$.

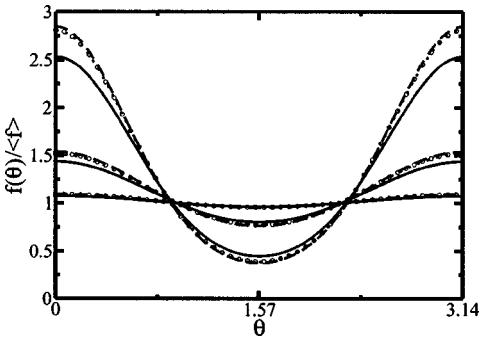

FIG. 10. Plot of the anisotropic factor of the finite cylinder, $f(\theta)/\langle f\rangle$, as a function of the tilt angle. The solid line is the result of the integration of Eq. (43) over the numerically computed surface charge on the cylinder. The circles are the result of the uniform model (see the text for details) while the dashed line is the result of the four parameter model described in the Appendix. The aspect ratio is $L/R=8$ and the screening factors are $\kappa_D R=0.2$, 0.5 and 1.0 (from bottom to top for $\theta=0$).

$$f(P)=1/\tilde{Z}\int\int_{\Sigma}\tilde{\sigma}(\mathbf{r}')\exp(-\kappa_D\mathbf{u}_r\cdot\mathbf{r}')dS'. \tag{43}$$

These ingredients can be therefore easily computed from the full numerical solution, once the auxiliary surface charge has been computed.

A. Total auxiliary charge

We show in Fig. 9 the size dependence of the total auxiliary charge $\tilde{Z}\ell_B/R$, for various screenings $\kappa_D R$. As can be seen in Fig. 9, the charge is mainly linear in L.

This result is compared with the predictions of the simplified models we have proposed in Sec. V. Within the simple uniform surface charge model described in Sec. V A, the total auxiliary charge reads

$$\tilde{Z}=2\pi RL\tilde{\sigma}_{\rm cyl}^{\rm uniform}+2\pi R^2\tilde{\sigma}_{\rm head}^{\rm uniform}. \tag{44}$$

Equation (41) reports the expressions of the *reduced* auxiliary charges (recall that in Sec. V, reduced variables have been used $\sigma^*=4\pi\ell_B R\sigma/e$). This leads eventually to the following expression of the total auxiliary charge as a function of the aspect ratio L/R and screening $\kappa_D R$:

$$\tilde{Z}\frac{\ell_B}{R}=\Phi_0\left\{\frac{1}{2}\frac{L}{R}\frac{1}{I_0(\kappa_D R)K_0(\kappa_D R)}+\frac{\kappa_D R}{1-e^{-\kappa_D R}}\times\left[1-\frac{1}{2I_0(\kappa_D R)}\right]\right\}. \tag{45}$$

This prediction is plotted as crosses on the previous figures, showing a relatively good agreement with the ''exact'' numerical results. The agreement might be slightly improved by considering the complete L dependence, while staying within the uniform model. This corresponds to solving the 2×2 system of equations, Eq. (38), with a numerical estimate of the Green functions for finite L. We have plotted the results of this approach as dotted lines in Fig. 9. This improves slightly the agreement especially for small L and $\kappa_D R$. We also present the results obtained using the ''four parameters'' model, described in the appendix. This model adds to the result in Eq. (44) the contribution of the rings which capture the edge effects. This model is not analytic either and as can be seen in Fig. 9, it does not improve much the agreement.

We conclude here that the very simple analytic expression in Eq. (44) provides a useful and trustworthy approximation for the total auxiliary charge which enters the interaction energy, Eq. (27).

B. Anisotropic terms

We report in Figs. 10 and 11 the numerical results for the anisotropic terms $f(P)$ for two cylinder sizes $L/R=8$ and $L/R=20$. These functions have been obtained after numerical integration of Eq. (43) using the numerical result for the auxiliary surface charge. In these figures, the anisotropic terms are plotted as a function of the tilt angle θ, between the axis z of the cylinder considered and the unit vector $\mathbf{u}$ linking the two cylinder centers (see, e.g., Fig. 3).

It is instructive to compare these ''exact'' anisotropic factors to the predictions of the simplified models for the surface charges discussed in Sec. V. Again, let us first concentrate on the uniform (auxiliary) charge model, proposed in Sec. V A. In the frame of this simplified description, the anisotropic factor, in Eq. (43), can be computed analytically

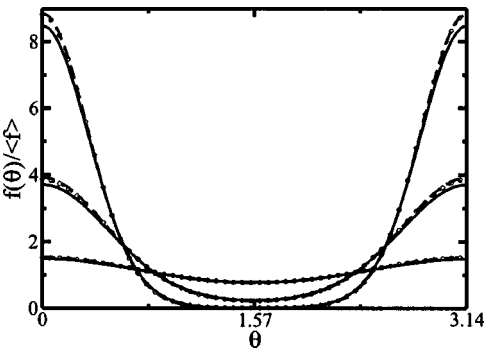

FIG. 11. Same as Fig. 10 but for an aspect ratio $L/R=20$.

since the auxiliary charges are constant over the head and the lateral side of the cylinder. This leads the following expression for $f(\theta)$:

$$f(\mathbf{n}) = \frac{\tilde{Z}_{\mathrm{cyl}}}{\tilde{Z}} f_{\mathrm{cyl}}(\theta) + \frac{\tilde{Z}_{\mathrm{head}}}{\tilde{Z}} f_{\mathrm{head}}(\theta), \tag{46}$$

where $\tilde{Z}_{\mathrm{cyl}} = 2\pi RL\tilde{\sigma}_{\mathrm{cyl}}$ is the total charge on the lateral sides of the polyelectrolyte, and $\tilde{Z}_{\mathrm{head}} = 2\pi R^2 \tilde{\sigma}_{\mathrm{head}}$ is the charge on the heads of the polyelectrolyte. Using Eq. (41) obtained within the uniform model one has

$$\begin{aligned} \tilde{Z}_{\mathrm{cyl}} \frac{\ell_B}{R} &= \frac{1}{2}\frac{L}{R}\Phi_0 \frac{1}{I_0(\kappa_D R) K_0(\kappa_D R)}, \\ \tilde{Z}_{\mathrm{head}} \frac{\ell_B}{R} &= \frac{\kappa_D R \Phi_0}{1 - e^{-\kappa_D R}} \left[1 - \frac{1}{2 I_0(\kappa_D R)} \right] \end{aligned} \tag{47}$$

and the total charge $\tilde{Z}$ is given in Eq. (45). On the other hand, the expressions for anistropic factors due to the cylinder and due to the heads read

$$\begin{aligned} f_{\mathrm{cyl}}(\theta) &= I_0(\kappa_D R \sin\theta) \frac{\sinh\left(\frac{\kappa_D L \cos\theta}{2} \right)}{\left(\frac{\kappa_D L \cos\theta}{2} \right)}, \\ f_{\mathrm{head}}(\theta) &= \frac{2 I_1(\kappa_D R \sin\theta)}{\kappa_D R \sin\theta} \cosh\left(\frac{\kappa_D L \cos\theta}{2} \right). \end{aligned} \tag{48}$$

This expression for $f(\theta)$, using the previous expressions for $\tilde{Z}_{\mathrm{cyl}}$ and $\tilde{Z}_{\mathrm{head}}$, is plotted against the numerical results in Figs. 10 and 11 for two aspects ratios ($L/R = 8$ and $L/R = 20$, respectively). The agreement is seen to be surprisingly good in view of the simplicity of the modelization.

In these figures, we also show the prediction of the more detailed ''four parameters'' model, which includes a crude description of the edge effect, as detailed in the Appendix. This approach adds a contribution from the rings to the previous anisotropic factors,

$$\frac{\tilde{Z}_{\mathrm{ring}}}{\tilde{Z}} f_{\mathrm{ring}}(\theta),$$

where $\tilde{Z}_{\mathrm{ring}} = 2 \times 2\pi R \ell (\tilde{\sigma}_3 + \tilde{\sigma}_4)$ is the total charge on the rings (see the Appendix for details). The contribution to the anisotropic factor due to the ring, f_{ring}, reads explicitly:

$$f_{\mathrm{ring}}(\theta) = I_0(\kappa_D R \sin\theta) \cosh\left(\frac{\kappa_D L \cos\theta}{2} \right). \tag{49}$$

As can be seen in the figures, this more detailed description does not improve much the agreement compared to the much simpler ''uniform'' approach.

Such a good agreement using a very simple description of the surface charge calls for some comments. The crucial point is that the interaction energy involves the *auxiliary* charges and not the bare charges. The full numerical resolution shows in fact that the edge effect is much more marked for the auxiliary charges than for the ''bare'' charge, in the sense that the divergence of the surface charge occurs much closer to the edge for the auxiliary charge. We have discussed this effect in Sec. IV D 1. As a result, the auxiliary charge profile is more flat than the ''real'' charge profile. This feature allows one to understand why the uniform model yields results in good agreement with the numerical results for the anisotropic factors.

VII. CONCLUSION

In the present paper, we have proposed a framework allowing one to generalize the DLVO interaction for anistropic macromolecules. The central result is the electrostatic interaction energy between two anistropic macromolecules

$$U_{12}(r) = \frac{\tilde{Z}_1 \tilde{Z}_2 f_1(\mathbf{u}_1) f_2(\mathbf{u}_2) e^{-\kappa_D r}}{4\pi\epsilon r}. \tag{50}$$

The main point resulting from Eq. (50) is that in a medium with finite salt concentration, the anisotropy is remanent at all distances. We have quantified this effect and obtained general formulas for the anisotropic factor $f(\mathbf{u}, \varphi)$ (which only depends on $\mathbf{u}$ for axisymmetrical objects) in Eq. (20). We have then applied this framework to finite rod-like cylinders. The previous calculations provide a simple and efficient description of the interaction between two such polyelectrolytes. In particular, the simple uniform model leads to an analytic expression for the total auxiliary charge and anisotropic terms which enter the interaction energy, that turn out to be in good agreement with the full numerical solution. With this approximation, the anisotropic factor $f(\mathbf{u})$ for a finite-size cylinder of length L and radius R at fixed potential Φ_0 takes a simple form

$$f(\mathbf{u}) = \frac{\tilde{Z}_{\mathrm{cyl}}}{\tilde{Z}} f_{\mathrm{cyl}}(\theta) + \frac{\tilde{Z}_{\mathrm{head}}}{\tilde{Z}} f_{\mathrm{head}}(\theta). \tag{51}$$

In the above expression, the auxiliary charges $\tilde{Z}_{\mathrm{cyl}}$, $\tilde{Z}_{\mathrm{head}}$, and $\tilde{Z}$, as well as the anisotropy factors $f_{\mathrm{cyl}}(\theta)$ and $f_{\mathrm{head}}(\theta)$ are given by

$$\begin{aligned} \tilde{Z}_{\mathrm{cyl}} \frac{\ell_B}{R} &= \frac{1}{2}\frac{L}{R}\Phi_0 \frac{1}{I_0(\kappa_D R) K_0(\kappa_D R)}, \\ \tilde{Z}_{\mathrm{head}} \frac{\ell_B}{R} &= \frac{\kappa_D R \Phi_0}{1 - e^{-\kappa_D R}} \left[1 - \frac{1}{2 I_0(\kappa_D R)} \right], \\ \tilde{Z} &= \tilde{Z}_{\mathrm{cyl}} + \tilde{Z}_{\mathrm{head}} \end{aligned}$$

and

$$\begin{aligned} f_{\mathrm{cyl}}(\theta) &= I_0(\kappa_D R \sin\theta) \frac{\sinh\left(\frac{\kappa_D L \cos\theta}{2} \right)}{\left(\frac{\kappa_D L \cos\theta}{2} \right)}, \\ f_{\mathrm{head}}(\theta) &= \frac{2 I_1(\kappa_D R \sin\theta)}{\kappa_D r_0 \sin\theta} \cosh\left(\frac{\kappa_D L \cos\theta}{2} \right). \end{aligned}$$

As will be shown in Ref. 19, the above expressions with the relevant choice of Φ_0 almost correspond to the interaction energy of two highly charged colloids far away from each other, *irrespective of their bare charge*.

A few further comments are in order.

First, the interaction energy, at a *fixed center to center distance between the two cylinders*, is found to be minimum when the tilt angle (made between each cylinder and the center to center direction) is equal to $\pi/2$, i.e., when both cylinders' axis are perpendicular to the center to center vector. Apart from that, the angle between the two axis of the cylinders is not constrained, at this level of approximation (the two axis may equally be perpendicular or parallel). This is a consequence of retaining only the leading order contribution in the potential, and higher order terms [in $\exp(-\kappa_D r)/r^i$ with $i>1$] would split the aforementioned degeneracy, and clearly stabilize the crossed rods compared to the parallel situation. On the other hand, the interaction is maximized when the two rods are coaxial (vanishing tilt angle). This result somehow contrasts with the infinite rod situation,[15] for which the minimum energy situation corresponds to crossed rods (which is compatible with what we found), but with a totally different angular dependence, and also a different distance dependence.

The anisotropic term in the interaction potential results in a coupling between orientational and translational degrees of freedom. The strength of this anisotropy is moreover found to increase with salt concentration. These ingredients suggest that at high salinity, frustrated phases might form, independently of van der Waals forces. However a full exploration of the phase diagram of charged rods using these previous results is required before reaching a definite conclusion on the formation of gels in rod-like systems at large salt concentrations, as seen experimentally.[6,8,9]

Work along these lines is in progress.

ACKNOWLEDGMENT

We would like to thank Miguel Aubouy for inspiring discussions and an enjoyable collaboration on related topics.

APPENDIX: A SIMPLE DESCRIPTION OF THE EDGE EFFECT

1. General framework

In this Appendix a more detailed description of the edge effect is proposed. We extend the model described in Sec. V A by incorporating a specific charge on the edge of the rod-like macromolecule. More specifically, we model the *auxiliary* surface charge as the superposition of a uniform charge on the head and on the lateral surface of the cylinder, supplemented by a ring charge on the edge of the macromolecule, as shown in Fig. 12.

From a technical point of view, we separate the ring charge on the edge of the molecule as a ring of radius R on the head, and a ring of radius R on the lateral side of the cylinder (see Fig. 12). The extension of the lateral ring is denoted as $\ell_{\rm cyl}$, and that on the edge $\ell_{\rm head}$. There are therefore *four parameters* in the model: respectively, the uniform surface charge on the head $\tilde{\sigma}_{\rm head}$, on the lateral sides $\tilde{\sigma}_{\rm cyl}$, $\tilde{\sigma}_{\rm cyl\ edge}$, and $\tilde{\sigma}_{\rm head\ edge}$. In the following results, we have chosen $\ell_{\rm cyl}=\ell_{\rm head}=0.05R$. Results are only weakly dependent on this choice. As in Sec. V A, one has to solve Eq. (30), relating the auxiliary surface charge to the potential Φ_0.

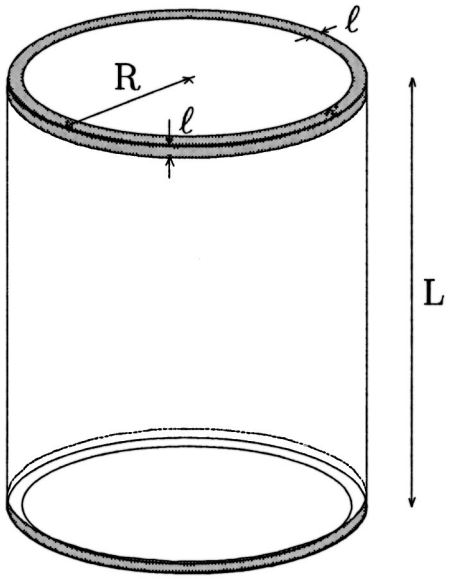

FIG. 12. Simplified description of the edge effects.

Within the simplified analysis, and taking into account the symmetry of the cylinder, this equation reduces to a 4×4 inversion: irrespective of j,

$$\sum_i \tilde{\sigma}_i \tilde{G}_{ij} = \Phi_0, \tag{A1}$$

where the summation i runs overs the different parts of the simplified object, e.g., $i=1$ stands for the center of the heads of the cylinder; $i=2$ stands for the middle part of the cylinder; while $i=3$ and $i=4$ stand for the rings on the edges. The "Green functions" $\tilde{G}_{ij}$ are defined in terms of the Green functions $G_{\rm disk}$, $G_{\rm cyl}$, and $G_{\rm ring}$ whose expressions are given, respectively, in Eqs. (31), (34), and (35) (see the following for the detailed expressions of the 4×4 matrix $\tilde{G}_{ij}$). Once the auxiliary charges $\tilde{\sigma}_i$ are known, one obtains the "bare" charge σ *everywhere* on the cylinder using Eq. (10). This can be written formally:

$$\sigma(\mathbf{r}) = \sum_i \tilde{\sigma}_i \frac{\partial \tilde{G}(\mathbf{r},i)}{\partial \mathbf{n}}, \tag{A2}$$

where the notation $\tilde{G}(\mathbf{r},i)$ stands for the Green function computed at point $\mathbf{r}$ due to charge i defined earlier; $\partial/\partial\mathbf{n}$ denotes the derivative along the normal to the surface at point $\mathbf{r}$.

Equation (A1) is easily inverted and the corresponding surface charges are plotted in the previous figures, Figs. 7 and 8. As shown on these plots, the approximate description yields results in excellent agreement with the full numerical resolution for any aspect ratio L/R and screening $\kappa_D R$.

As a consequence, despite its simplicity, the simplified description of the auxiliary charges contains most of the physics of the edge effect. Also, as shown by the previous argument, a better agreement is expected for large $\kappa_D R$.

2. Technical details

The cylinder is decomposed into four different pieces:

(1) a lateral part of length L and radius R,
(2) two disks of radius R,
(3) two lateral rings of radius R, of heights ℓ_{cyl}, and of centers located in $[0,\pm(L/2\mp\ell_{\mathrm{cyl}}/2)]$,
(4) two rings of radius $R-\ell_{\mathrm{head}}/2$ and widths ℓ_{head},

respectively, denoted 1, 2, 3, and 4 and carrying the uniform surface charge densities $\tilde{\sigma}_{\mathrm{cyl}}$, $\tilde{\sigma}_{\mathrm{head}}$, $\tilde{\sigma}_{\mathrm{cyl\ edge}}$, and $\tilde{\sigma}_{\mathrm{head\ edge}}$. To simplify the formulation of the equations, we respectively call $G_{\mathrm{cyl}}(r_0,r,\ell,z)$ and $G_{\mathrm{ring}}(r_0,\ell_{\mathrm{head}},r,z)$ the electrostatic potentials by a cylinder of radius r_0 and of height ℓ located in (r,z) and by a ring of radius r_0 and of width ℓ_{head} in (r,z) with the origin of the coordinates (0,0) located in the center of the cylinder or of the ring.

In order to find the auxiliary charges on the disks, rings, and lateral sides of the cylinder, one has to solve the 4×4 linear problem, obtained from Eq. (30):

$$\forall j\in\{1,2,3,4\},\quad \sum_i \tilde{\sigma}_i A_{ij}=\Phi_0.$$

The coefficients A_{ij} are given in terms of the expressions of G_{cyl} and G_{disk} given in Eqs. (34) and (35):

$$\begin{aligned}
&A_{11}=G_{\mathrm{cyl}}(R,R,L,0),\\
&A_{12}=2G_{\mathrm{disk}}(R,R,L/2),\\
&A_{13}=2G_{\mathrm{cyl}}(R,R,\ell_{\mathrm{cyl}},L/2-\ell_{\mathrm{cyl}}/2),\\
&A_{14}=2G_{\mathrm{ring}}(R-\ell_{\mathrm{head}}/2,R,L/2),
\end{aligned}\tag{A3}$$

$$\begin{aligned}
&A_{21}=G_{\mathrm{cyl}}(R,0,L,L/2),\\
&A_{22}=G_{\mathrm{disk}}(R,R,0)+G_{\mathrm{disk}}(R,0,L),\\
&A_{23}=G_{\mathrm{cyl}}(R,0,\ell_{\mathrm{cyl}},\ell_{\mathrm{cyl}}/2)+G_{\mathrm{cyl}}(R,0,\ell_{\mathrm{cyl}},L-\ell_{\mathrm{cyl}}/2),\\
&A_{24}=G_{\mathrm{ring}}(R-\ell_{\mathrm{head}}/2,0,0)+G_{\mathrm{ring}}(R-\ell_{\mathrm{head}}/2,0,L),
\end{aligned}\tag{A4}$$

$$A_{31}=G_{\mathrm{cyl}}(R,R,L,L/2-\ell_{\mathrm{cyl}}/2),\tag{A5}$$

$$\begin{aligned}
&A_{32}=G_{\mathrm{disk}}(R,R,\ell_{\mathrm{cyl}}/2)+G_{\mathrm{disk}}(R,R,L-\ell_{\mathrm{cyl}}/2),\\
&A_{33}=G_{\mathrm{cyl}}(R,R,\ell_{\mathrm{cyl}}/2,0)+G_{\mathrm{cyl}}(R,R,L-\ell_{\mathrm{cyl}}),
\end{aligned}\tag{A6}$$

$$\begin{aligned}
&A_{34}=G_{\mathrm{ring}}(R-\ell_{\mathrm{head}}/2,R,\ell_{\mathrm{cyl}}/2)\\
&\qquad+G_{\mathrm{ring}}(R-\ell_{\mathrm{head}}/2,R,L-\ell_{\mathrm{cyl}}/2)),\\
&A_{41}=G_{\mathrm{cyl}}(R,R-\ell_{\mathrm{head}}/2,L,L/2),\\
&A_{42}=G_{\mathrm{disk}}(R,R-\ell_{\mathrm{head}}/2,0)+G_{\mathrm{disk}}(R,R-\ell_{\mathrm{head}}/2,L),\\
&A_{43}=G_{\mathrm{cyl}}(R,R-\ell_{\mathrm{cyl}}/2,\ell_{\mathrm{cyl}}/2)\\
&\qquad+G_{\mathrm{cyl}}(R,R-\ell_{\mathrm{cyl}}/2,L-\ell_{\mathrm{cyl}}/2),\\
&A_{44}=G_{\mathrm{disk}}(R-\ell_{\mathrm{head}}/2,R-\ell_{\mathrm{head}}/2,0)\\
&\qquad+G_{\mathrm{disk}}(R-\ell_{\mathrm{head}}/2,R-\ell_{\mathrm{head}}/2,L).
\end{aligned}\tag{A7}$$

Once the $\tilde{\sigma}$ have been calculated, we get σ using Eq. (36), which reads within the simplified description:

$$\forall i\in\{1,2,3,4\},\quad \sigma_i(\mathbf{r})=\sum_j \tilde{\sigma}_j B_{ij}(\mathbf{r}).\tag{A8}$$

The coefficients $B_{ij}(\mathbf{r})$ are given by

$$\begin{aligned}
&B_{11}(z)=\left(-\frac{\partial G_{\mathrm{cyl}}(R,r,L,z)}{\partial r}\right)_{R^+},\\
&B_{12}(z)=\left(-\frac{\partial G_{\mathrm{disk}}(R,r,L/2-z)}{\partial r}\right)_{R^+}\\
&\qquad+\left(-\frac{\partial G_{\mathrm{disk}}(R,r,L/2+z)}{\partial r}\right)_{R^+},\\
&B_{13}(z)=\left(-\frac{\partial G_{\mathrm{cyl}}(R,r,\ell_{\mathrm{cyl}},L/2-\ell_{\mathrm{cyl}}/2-z)}{\partial r}\right)_{R^+}\\
&\qquad+\left(-\frac{\partial G_{\mathrm{cyl}}(R,r,\ell_{\mathrm{cyl}},L/2-\ell_{\mathrm{cyl}}/2+z)}{\partial r}\right)_{R^+},\\
&B_{14}(z)=\left(-\frac{\partial G_{\mathrm{ring}}(R-\ell_{\mathrm{head}}/2,r,L/2-z)}{\partial r}\right)_{R^+}\\
&\qquad+\left(-\frac{\partial G_{\mathrm{ring}}(R-\ell_{\mathrm{head}}/2,r,L/2+z)}{\partial r}\right)_{R^+},
\end{aligned}\tag{A9}$$

$$\begin{aligned}
&B_{21}(r)=\left(-\frac{\partial G_{\mathrm{cyl}}(R,r,L,z)}{\partial z}\right)_{L/2^+},\\
&B_{22}(r)=\frac{1}{2}+\left(-\frac{\partial G_{\mathrm{disk}}(R,r,z)}{\partial z}\right)_{L^+},\\
&B_{23}(r)=\left(-\frac{\partial G_{\mathrm{cyl}}(R,r,\ell_{\mathrm{cyl}},\ell_{\mathrm{cyl}}/2)}{\partial z}\right)_{\ell_{\mathrm{cyl}}/2^+}\\
&\qquad+\left(-\frac{\partial G_{\mathrm{cyl}}(R,r,\ell_{\mathrm{cyl}},z)}{\partial z}\right)_{(L-\ell_{\mathrm{cyl}}/2)^+},\\
&B_{24}(r)=\frac{1_{\mathrm{ring}}(r)}{2}+\\
&\qquad\left(-\frac{\partial G_{\mathrm{ring}}(R-\ell_{\mathrm{head}}/2,r,z)}{\partial z}\right)_{(L-\ell_{\mathrm{cyl}}/2)^+},
\end{aligned}\tag{A10}$$

with $1_{\mathrm{ring}}(r)=1$ if $R-\ell_{\mathrm{head}}\leqslant r\leqslant R$ and 0 otherwise,

$$\begin{aligned}
&B_{31}=\left(-\frac{\partial G_{\mathrm{cyl}}(R,r,L,L-\ell_{\mathrm{cyl}}/2)}{\partial r}\right)_{R^+},\\
&B_{32}=\left(-\frac{\partial G_{\mathrm{disk}}(R,r,\ell_{\mathrm{cyl}}/2)}{\partial r}\right)_{R^+}\\
&\qquad+\left(-\frac{\partial G_{\mathrm{disk}}(R,r,L-\ell_{\mathrm{cyl}}/2)}{\partial r}\right)_{R^+},\\
&B_{33}=\left(-\frac{\partial G_{\mathrm{cyl}}(R,r,\ell_{\mathrm{cyl}}/2,0)}{\partial r}\right)_{R^+}\\
&\qquad+\left(-\frac{\partial G_{\mathrm{cyl}}(R,r,\ell_{\mathrm{cyl}},L-\ell_{\mathrm{cyl}})}{\partial r}\right)_{R^+},
\end{aligned}\tag{A11}$$

$$
\begin{aligned}
B_{34} &= \left(-\frac{\partial G_{\mathrm{ring}}(R-\ell_{\mathrm{head}}/2, r, \ell_{\mathrm{cyl}}/2)}{\partial r} \right)_{R^+} \\
&\quad + \left(-\frac{\partial G_{\mathrm{ring}}(R-\ell_{\mathrm{head}}/2, r, L-\ell_{\mathrm{cyl}}/2)}{\partial r} \right)_{R^+}, \\
B_{41} &= \left(-\frac{\partial G_{\mathrm{cyl}}(R, R-\ell_{\mathrm{head}}/2, L, z)}{\partial z} \right)_{L/2^+}, \\
B_{42} &= \frac{1}{2} + \left(-\frac{\partial G_{\mathrm{disk}}(R, R-\ell_{\mathrm{head}}/2, L)}{\partial z} \right)_{L}, \\
B_{43} &= \left(-\frac{\partial G_{\mathrm{cyl}}(R, R-\ell_{\mathrm{head}}/2, \ell_{\mathrm{cyl}}, \ell_{\mathrm{cyl}}/2)}{\partial z} \right)_{\ell_{\mathrm{cyl}}/2^+} \\
&\quad + \left(-\frac{\partial G_{\mathrm{cyl}}(R, R-\ell_{\mathrm{head}}/2, \ell_{\mathrm{cyl}}, L-\ell_{\mathrm{cyl}}/2)}{\partial z} \right)_{(L-\ell_{\mathrm{cyl}}/2)^+}, \\
B_{44} &= \frac{1}{2} + \left(-\frac{\partial G_{\mathrm{ring}}(R-\ell_{\mathrm{head}}/2, R-\ell_{\mathrm{head}}/2, L)}{\partial z} \right)_{L^+}.
\end{aligned}
\tag{A12}
$$

[1] E. J. W. Verwey and J. T. G. Overbeek, *Theory of the Stability of Lyophobic Colloids* (Elsevier, Amsterdam, 1948).
[2] J. C. Crocker and D. G. Grier, Phys. Rev. Lett. **73**, 352 (1994).
[3] S. Fraden, G. Maret, D. L. D. Caspar, and R. B. Meyer, Phys. Rev. Lett. **63**, 2068 (1989).
[4] K. R. Purdy, Z. Dogic, S. Fraden, A. Rühm, L. Lurio, and S. G. J. Mochrie, Phys. Rev. E **67**, 031708 (2003).
[5] B. Guilleaume, J. Blaul, M. Ballauff, M. Witteman, M. Rehahn, and G. Goerigk, Eur. Phys. J. E **8**, 299 (2002).
[6] P. A. Buining, A. P. Philippse, and H. N. W. Lekkerkerker, Langmuir **10**, 2106 (1994).
[7] O. Pelletier, P. Davidson, C. Bourgaux, and J. Livage, Europhys. Lett. **48**, 53 (1999).
[8] A. Mourchid, A. Delville, J. Lambard, E. Lécolier, and P. Levitz, Langmuir **11**, 1942 (1995).
[9] A. Mourchid, E. Lécolier, H. van Damme, and P. Levitz, Langmuir **14**, 4718 (1998).
[10] T. Nicolai and S. Coccard, Eur. Phys. J. E **5**, 221 (2001).
[11] D. van der Beer and H. N. W. Lekkerkerker, Europhys. Lett. **61**, 702 (2003).
[12] I. Langmuir, J. Chem. Phys. **6**, 873 (1938).
[13] T. Odijk, Macromolecules **19**, 9 (1986).
[14] L. Onsager, Ann. N.Y. Acad. Sci. **51**, 627 (1949).
[15] A. Stroobants, H. N. W. Lekkerkerker, and T. Odijk, Macromolecules **19**, 2232 (1986).
[16] D. Bonn, H. Kellay, H. Tanaka, G. Wedgam, and J. Meunier, Langmuir **15**, 7534 (1999).
[17] E. Trizac, L. Bocquet, R. Agra, J.-J. Weiss, and M. Aubouy, J. Phys.: Condens. Matter **14**, 9339 (2002).
[18] J. D. Jackson, *Classical Electrodynamics* (Wiley, New York, 1975).
[19] D. Chapot, L. Bocquet, and E. Trizac (unpublished).
[20] L. Bocquet, E. Trizac, and M. Aubouy, J. Chem. Phys. **117**, 8138 (2002).
[21] E. Trizac, Phys. Rev. E **62**, R1465 (2000).
[22] R. J. F. Leote de Carvalho, E. Trizac, and J. P. Hansen, Phys. Rev. E **61**, 1634 (2000).